

Itinerant antiferromagnetism in BaCr₂As₂

D.J. Singh, A.S. Sefat, M.A. McGuire, B.C. Sales, and D. Mandrus

Materials Science and Technology Division, Oak Ridge National Laboratory, Oak Ridge, Tennessee 37831-6114

L.H. VanBebber and V. Keppens

*Department of Materials Science and Engineering,
The University of Tennessee, Knoxville, TN 37996-2200*

(Dated: August 3, 2021)

We report single crystal synthesis, specific heat and resistivity measurements and electronic structure calculations for BaCr₂As₂. This material is a metal with itinerant antiferromagnetism, similar to the parent phases of Fe-based high temperature superconductors, but differs in magnetic order. Comparison of bare band structure density of states and the low temperature specific heat implies a mass renormalization of ~ 2 . BaCr₂As₂ shows stronger transition metal - pnictogen covalency than the Fe compounds, and in this respect is more similar to BaMn₂As₂. This provides an explanation for the observation that Ni and Co doping is effective in the Fe-based superconductors, but Cr or Mn doping is not.

PACS numbers: 75.10.Lp, 71.20.Lp, 74.70.Dd

I. INTRODUCTION

The discovery of high temperature Fe-based superconductivity¹ has resulted in substantial activity leading to the finding of a wide range of Fe-based superconductors, including a number of materials in the ThCr₂Si₂ structure, prototype BaFe₂As₂.² Similar to the oxy-arsenides, BaFe₂As₂ is metallic and shows spin density wave (SDW) antiferromagnetism when cooled.³ BaFe₂As₂ becomes superconducting when the SDW is destroyed, either by doping with holes² or electrons,⁴ or by using pressure.⁵ In fact, it is remarkable that superconductivity can be induced by doping on the Fe-site, using Co and Ni as electron dopants.^{4,6} This is in contrast to the behavior observed in cuprate superconductors, where alloying on the Cu site strongly suppresses superconductivity.

The electronic structure of BaFe₂As₂ is similar to the other iron based superconducting materials in that the Fermi energy (E_F) lies in at the bottom of a pseudogap in the electronic density of states. The corresponding Fermi surface then consists of small disconnected hole and electron pockets around the zone center and zone corner.^{7,8,9,10} Importantly the bands within 2 eV of the Fermi energy arise from Fe d states with only modest As p hybridization. BaCo₂As₂ and BaNi₂As₂, show very different properties, namely those of a material very close to ferromagnetism,¹¹ and a low temperature electron-phonon superconductor, respectively.^{12,13,14} Importantly, however, the electronic structures of BaT₂As₂, $T=\text{Fe,Co,Ni}$, are closely related, with Fe d bands near E_F , modest hybridization with As, and a similar shaped density of states with a pseudogap at an electron count of six d electrons. The main differences in physical properties are due to the different electron counts of Fe²⁺, Co²⁺ and Ni²⁺. This common behavior also is thought to be important for the superconductivity in the Co-doped superconductor BaFe_{2-x}Co_xAs₂, whose electronic struc-

ture behaves as a coherent alloy.⁴ On the other hand, to our knowledge, superconductivity has not been reported in BaFe₂As₂ doped with Mn or Cr so far. BaMn₂As₂ shows an electronic structure very different from the $T=\text{Fe,Co,Ni}$ compounds. In particular, it has strong spin dependent hybridization between Mn d states and As p states, and is a small band gap semiconductor with a high exchange couplings and ordering temperature that result from the strong hybridization.^{15,16} Here we report investigation of the $T=\text{Cr}$ material, BaCr₂As₂. This material is known to form in the ThCr₂Si₂ structure,¹⁷ but little has been reported about its physical properties. We find that similar to BaMn₂As₂ it has strong spin dependent Cr d - As p hybridization, but unlike that material it is a renormalized antiferromagnetic metal, with a G -type (checkerboard) order and very strong magnetic interactions.

II. METHODS

BaCr₂As₂ single crystals were prepared starting from high purity elements ($> 99.9\%$, source Alfa Aesar). The crystals were grown out of CrAs binary. Cr powder and As pieces were reacted slowly by heating to 300 °C (50 °C/hr, dwell 10 hrs), to 600 °C (30 °C/hr dwell 30 hrs), then to 900 °C (30 °C/hr, dwell 24 hrs). A ratio of Ba:CrAs = 1:4 was heated for 13 hours at 1230 °C under partial argon atmosphere. The ampule was cooled at the rate of 2 °C/hr, followed by decanting of flux at 1120 °C. Electron probe microanalysis of a cleaved surface of the single crystal was performed on a JEOL JSM-840 scanning electron microscope using an accelerating voltage of 15 kV and a current of 20 nA with an EDAX brand energy-dispersive X-ray spectroscopy (EDS) device. EDS analyses on the crystal indicated a Ba:Cr:As ratio of 1:2:2, within the error bars. The phase purity of the crystals was determined using a Scintag XDS 2000 2 θ -

2 Θ diffractometer (Cu K_α radiation). BaCr₂As₂ crystallizes with the ThCr₂Si₂ structure at room temperature (tetragonal spacegroup $I4/mmm$, No. 139, $Z=2$). Lattice constants were determined from LeBail refinements using the program FullProf.¹⁸ The resulting room temperature lattice parameters were $a=3.9678(4)$ Å, $c=13.632(3)$ Å.

Temperature dependent electrical resistivity measurements were performed on a Quantum Design Physical Property Measurement System (PPMS). The electrical contacts were placed on the samples in the standard 4-probe geometry, using Pt wires and silver paste. The resistivity was measured in the ab -plane, i.e. $\rho_{ab}(T)$. Specific heat data, $C_p(T)$, were also obtained using the PPMS. The relaxation method was used from 2 K to 200 K.

The first principles calculations were done within the local density approximation (LDA) using the general potential linearized augmented planewave (LAPW) method,¹⁹ similar to prior calculations for BaFe₂As₂.⁷ We used the reported experimental lattice parameters from literature,¹⁷ $a=3.963$ Å, $c=13.600$ Å, which are very close to the room temperature values determined here. The internal parameter, z_{As} was determined by energy minimization. The resulting value for the lowest energy G-type antiferromagnetic ordering is $z_{As}=0.3572$. This value shows sensitivity to magnetic order as in the Fe-based compounds.²⁰ A relaxation for ferromagnetic order yielded $z_{As}=0.3526$. We used well converged basis sets, including local orbitals to treat the semi-core states and relax the Cr d state linearization.²¹ Relativistic effects were included at the scalar relativistic level. The LAPW sphere radii were $2.2 a_0$ for Ba and $2.1 a_0$ for Cr and As.

III. DENSITY FUNCTIONAL CALCULATIONS

We begin with a discussion of the magnetic order. We calculated the energy as a function of magnetic ordering for different likely configurations. These were a non-spin-polarized calculation (i.e. no magnetism), and three magnetic orderings of the Fe planes, with both ferromagnetic and antiferromagnetic layer stackings for each. These orders were ferromagnetic, checkerboard nearest neighbor antiferromagnetism and a magnetic structure consisting of ferromagnetic chains of nearest neighbor Fe, alternating antiferromagnetically, as in the SDW state of the undoped Fe superconducting materials. The results are summarized in Table I. As may be seen, checkerboard order with antiferromagnetic stacking, i.e. G-type antiferromagnetism, yields the lowest energy. This state has a Cr moment of $\sim 2 \mu_B$.

Turning to the details, one may note that although the magnetic energy is large, ~ -0.2 eV / Cr for the ground state, and all the magnetic ordering patterns tested are lower energy than the non-spin-polarized case, the differences between different orderings are of almost the same scale. For example, the difference between the chain-like

TABLE I: LDA magnetic energy, E_{mag} of BaCr₂As₂. The energies are given for $z_{As}=0.3572$, on a per formula unit basis (two Cr atoms) with respect to the non-spin-polarized energy. The moments, m_{Cr} are the spin moments defined by the integral over the Cr LAPW sphere. The notation for the magnetic order is as follows: P denotes non-spin-polarized, otherwise the first letter denotes the in-plane magnetic order (F for ferromagnetic, C for checkerboard nearest neighbor antiferromagnetism, and S for chains of like-spin Fe, as in the SDW of the Fe-based compounds), and the second denotes either antiferromagnetic stacking (A) or ferromagnetic stacking (F) along the c -axis.

Magnetic Order	E_{mag} (eV)	m_{Cr} (μ_B)
P	0.000	0.00
F-F	-0.157	1.56
F-A	-0.146	1.51
S-F	-0.059	1.73
S-A	-0.058	1.80
C-F	-0.382	2.05
C-A	-0.394	2.01

order (S-A) that is the ground state for the Fe-based superconductors and the G-type ground state of BaCr₂As₂ is 0.17 eV/Cr, i.e. $\sim 85\%$ of the magnetic energy in the ground state. This implies that the magnetism has significant itinerant character, in the sense that band structure (hopping) is important in the moment formation, as opposed to just atomic physics, with hopping important only in the inter-site exchange. Also, one may note that the c -axis coupling is small compared to the in-plane coupling, and is antiferromagnetic for the ground state, but that the sign depends on the details of the in-plane order, implying that more than nearest neighbor interactions are important. This is also apparent from the in-plane energetics. A simple fit of the energies for antiferromagnetic stacking to a Heisenberg model with nearest neighbor (J_1) and next nearest neighbor (J_2) interactions, would yield antiferromagnetic J_1 and a large opposite (ferromagnetic) J_2 , $J_2/J_1=-0.85$. The large magnitude of J_2 implies that this model is probably not reliable and that the interactions are probably long range, as might be expected in a metal with itinerant magnetism.

The main results for the LDA electronic structure are given in Figs. 1, 2 and 3, which show the electronic density of states (DOS), the band structure and the Fermi surface, respectively for the G-type ground state order. Fig. 1 shows in addition the DOS for a ferromagnetic order. The compound is metallic for either order.

An examination of the DOS shows that the states near the E_F are hybridized Cr d - As p combinations and that the hybridization is spin-dependent. This is similar to BaMn₂As₂, but rather different from the $T=Fe, Co, Ni$ series where, as mentioned, the states near E_F are dominated by d character. In analyzing the DOS, it is important to keep in mind that the projections in the LAPW method are onto the LAPW spheres. Since a Cr $3d$ orbital is almost entirely contained within a $2.1 a_0$ sphere,

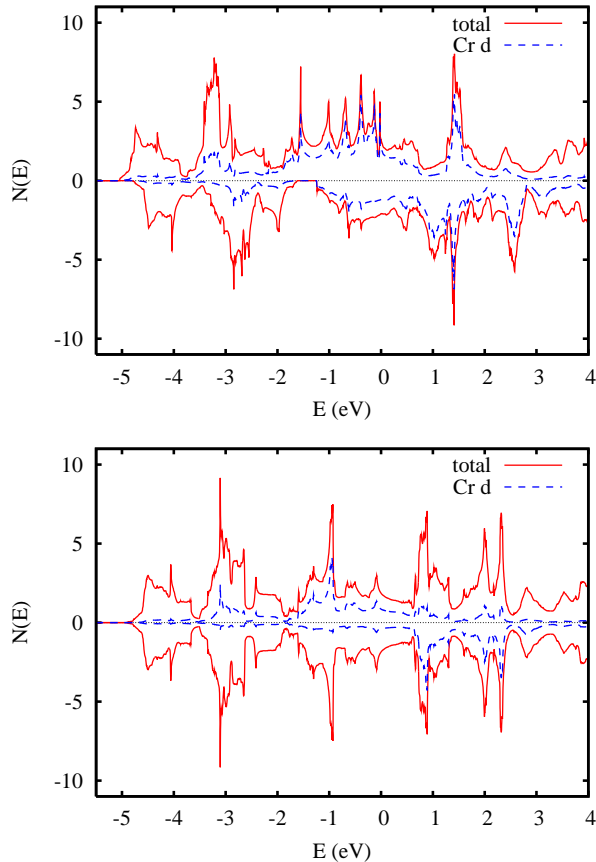


FIG. 1: Calculated electronic density of states BaCr_2As_2 with ferromagnetic (top) and nearest neighbor antiferromagnetic (bottom) ordering. Majority spin is shown above the axis and minority spin below. The projection is onto the LAPW sphere, radius $2.1 a_0$. In the top panel the Cr projections are for both atoms. In the bottom panel, spin up and spin down are identical, and the projections shown are majority and minority spin for one Cr atom. The total DOS is per formula unit.

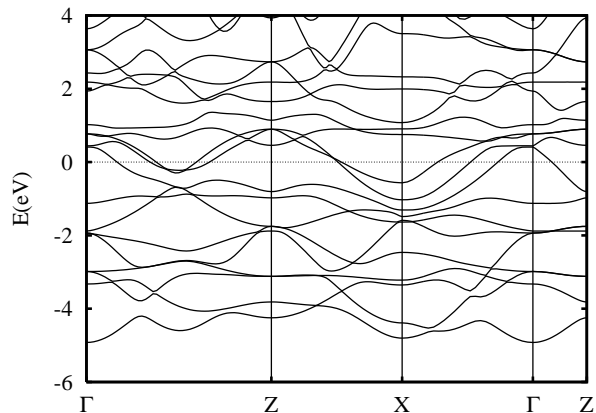


FIG. 2: Calculated band structure of BaCr_2As_2 with nearest neighbor antiferromagnetic ordering.

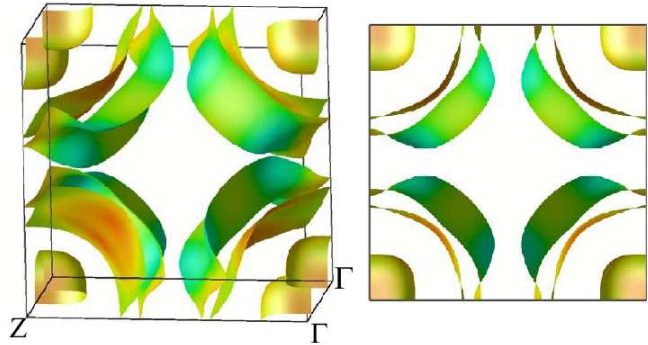


FIG. 3: (color online) Calculated extended zone Fermi surface of antiferromagnetic BaCr_2As_2 , showing a view off the c -axis (left) and along the c -axis (right). The shading is by velocity.

the Cr d projection is a reasonable approximation to the Cr d contribution to the DOS. However, As p states are extended and would have substantial weight outside a sphere of this radius. Thus when considering the electronic structure, the difference between the total DOS and the Cr d projection is a better measure of the As p contribution than the As p projection, which would underestimate the As contribution. Viewed in this way, As p orbitals contribute approximately 1/3 of the DOS at E_F and furthermore of the remaining 2/3, which is Cr d in character, the majority spin contributes more than twice as much as the minority spin. As may be seen comparing the top and bottom panels of Fig. 1, the details of this spin dependent hybridization are sensitive to the magnetic order. This explains the large energy differences between different magnetic orders.

As mentioned, BaCr_2As_2 is metallic. We find a large multisheet Fermi surface. This consists of small rounded electron cubes around Γ , and two electron cylinders, also centered at Γ and running along the k_z direction. The outermost cylinder in particular has significant corrugation.

The density of states at the Fermi energy is moderately high, $N(E_F)=3.7 \text{ eV}^{-1}$ on a per formula unit, both spins basis. This corresponds to a non-renormalized bare band specific heat coefficient $\gamma_0=9.3 \text{ mJ}/(\text{K}^2 \text{ mol})$. The calculated anisotropy is modest. The ab -plane and c -axis Fermi velocities are $\langle v_x^2 \rangle^{1/2}=2.08 \times 10^5 \text{ m/s}$ and $\langle v_z^2 \rangle^{1/2}=1.08 \times 10^5 \text{ m/s}$, respectively. If the scattering rate is isotropic this would correspond to $\rho_c/\rho_{ab}=4$. If the scattering rate is the same for all Fermi surfaces, c -axis conduction will be roughly equally from the small Γ centered pocket and the outer electron cylinder, while the in-plane conduction will come mostly from two cylinders.

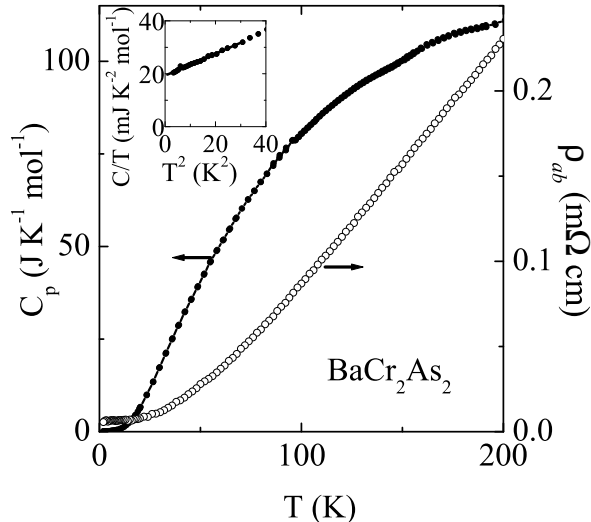


FIG. 4: Single crystal specific heat and resistivity of BaCr_2As_2 as a function of temperature. The inset shows the linear dependence of C/T vs. T^2 with finite value at $T = 0$.

IV. TRANSPORT AND SPECIFIC HEAT

Fig. 4 shows the temperature dependent resistivity and specific heat for a single crystal of BaCr_2As_2 . As mentioned, the resistivity was measured in the ab plane. As may be seen, the sample is clearly metallic with an increasing $\rho(T)$ and a finite $C_P(T)/T$ at low T . This is in accord with the results of our LDA calculations. There are no features suggesting a phase transition in either $\rho(T)$ or $C_P(T)$ from 2 K to 200 K. This is perhaps not surprising considering the large energy differences between different magnetic configurations found in the LDA calculations, as these differences would suggest an ordering temperature well above the maximum temperature

of our measurements. We find specific heat $\gamma=19.3(1)$ $\text{mJ}/(\text{K}^2 \text{ mol})$, i.e. $\sim 9.6 \text{ mJ}/(\text{K}^2 \text{ mol Cr})$. Comparing with the bare band structure value, we find an enhancement of $\gamma/\gamma_0 \sim 2$. This is a substantial renormalization, comparable to the Fe-based superconductors, although the physics in BaCr_2As_2 may be different. The renormalization may come in part from the electron-phonon interaction and in part from spin-fluctuations or other correlation effects.

V. SUMMARY AND CONCLUSIONS

We find that BaCr_2As_2 is an itinerant antiferromagnetic metal with a complex multisheet Fermi surface and substantial (~ 2) specific heat renormalization. While the electronic structure and magnetic order are different from those in the Fe-based superconducting materials, these results suggest that BaCr_2As_2 is an interesting material for further investigation. We also note that the stronger Cr-As covalency relative to the Fe-based superconductors means that Cr dopant atoms in those materials will produce more scattering than Co or Ni dopants, perhaps explaining why superconductivity has not yet been observed in Cr-doped BaFe_2As_2 . Finally, we note that BaMn_2As_2 and BaMn_2Sb_2 have been discussed as potential thermoelectric materials.^{15,22} The present results showing similar bonding with As and spin dependent metal - As bonding in the Cr compound as was found previously in the Mn compounds suggest that Cr could be used for doping studies of the thermoelectric properties of the Mn phases.

Acknowledgments

This work was supported by the Department of Energy, Division of Materials Sciences and Engineering and by the ORNL LDRD program.

¹ Y. Kamihara, T. Watanabe, M. Hirano, and H. Hosono, *J. Am. Chem. Soc.* **130**, 3296 (2008).
² M. Rotter, M. Tegel, and D. Jorendt, *Phys. Rev. Lett.* **101**, 107006 (2008).
³ M. Rotter, M. Tegel, D. Jorendt, I. Schellenberg, W. Hermes, and R. Pottgen, *Phys. Rev. B* **78**, 020503(R) (2008).
⁴ A. S. Sefat, R. Jin, M. A. McGuire, B. C. Sales, D. J. Singh, and D. Mandrus, *Phys. Rev. Lett.* **101**, 117004 (2008).
⁵ P. L. Alireza, Y. T. C. Ko, J. Gillett, C. M. Petrone, J. M. Cole, G. G. Lonzarich, and S. E. Sebastian, *J. Phys. Condens. Matter* **21**, 012208 (2009).
⁶ S. Matsuishi, Y. Inoue, T. Nomura, Y. Kamihara, M. Hirano, and H. Hosono, arXiv:0811.1147 (2008).
⁷ D. J. Singh, *Phys. Rev. B* **78**, 094511 (2008).
⁸ D. J. Singh and M. H. Du, *Phys. Rev. Lett.* **100**, 237003 (2008).

⁹ I. A. Nekrasov, Z. V. Pchelkina, and M. V. Sadovskii, *JETP Lett.* **88**, 144 (2008).
¹⁰ I. I. Mazin, D. J. Singh, M. D. Johannes, and M. H. Du, *Phys. Rev. Lett.* **101**, 057003 (2008).
¹¹ A. S. Sefat, D. J. Singh, R. Jin, M. A. McGuire, B. C. Sales, and D. Mandrus, *Phys. Rev. B* **79**, 024512 (2009).
¹² F. Ronning, N. Kurita, E. D. Bauer, B. L. Scott, T. Park, T. Klimczuk, R. Movshovich, and J. D. Thompson, *J. Phys. Condens. Matter* **20**, 342203 (2008).
¹³ N. Kurita, F. Ronning, Y. Tokiwa, E. D. Bauer, A. Subedi, D. J. Singh, J. D. Thompson, and R. Movshovich, arXiv:0811.3426 (2008).
¹⁴ A. Subedi and D. J. Singh, *Phys. Rev. B* **78**, 132511 (2008).
¹⁵ J. An, A. S. Sefat, D. J. Singh, and M. H. Du, arXiv:0901.0272 (2009).
¹⁶ Y. Singh, A. Ellern, and D. C. Johnston, arXiv:0901.3370

- (2009).
- ¹⁷ M. Pfisterer and G. Nagorsen, *Z. fur Naturforschung B* **35**, 703 (1980).
- ¹⁸ J. Rodriguez-Carvajal, FullProf Suite 2005, Version 3.30, June 2005, ILL.
- ¹⁹ D. J. Singh and L. Nordstrom, *Planewaves Pseudopotentials and the LAPW Method, 2nd Edition* (Springer, Berlin, 2006).
- ²⁰ I. I. Mazin, M. D. Johannes, L. Boeri, K. Koepernik, and D. J. Singh, *Phys. Rev. B* **78**, 085104 (2008).
- ²¹ D. Singh, *Phys. Rev. B* **43**, 6388 (1991).
- ²² H. F. Wang, K. F. Cai, H. Li, L. Wang, and C. W. Zhou, *J. Alloys Compds.* doi:10.1016/j.jallcom.2008.10.080 (2009).